Earth Syst. Sci. Data, 14, 5333–5347, 2022
https://doi.org/10.5194/essd-14-5333-2022

Open Access Earth System Science Data

Global land surface 250 m 8 d fraction of absorbed photosynthetically active radiation (FAPAR) product from 2000 to 2021

Han Ma[1], Shunlin Liang[1], Changhao Xiong[2], Qian Wang[3], Aolin Jia[4], and Bing Li[5]

[1]Department of Geography, The University of Hong Kong, Pokfulam, Hong Kong SAR, China
[2]School of Remote Sensing and Information Engineering, Wuhan University, Hubei 430010, China
[3]Faculty of Geography, Beijing Normal University, Beijing 100875, China
[4]Department of Geographical Sciences, University of Maryland, College Park, MD 20742, USA
[5]Key Research Institute of Yellow River Civilization and Sustainable Development & Collaborative Innovation Center on Yellow River Civilization of Henan Province, Henan University, Kaifeng 475001, China

Correspondence: Shunlin Liang (shunlin@hku.hk)

Received: 14 April 2022 – Discussion started: 2 August 2022
Revised: 2 November 2022 – Accepted: 2 November 2022 – Published: 7 December 2022

Abstract. The fraction of absorbed photosynthetically active radiation (FAPAR) is a critical land surface variable for carbon cycle modeling and ecological monitoring. Several global FAPAR products have been released and have become widely used; however, spatiotemporal inconsistency remains a large issue for the current products, and their spatial resolutions and accuracies can hardly meet the user requirements. An effective solution to improve the spatiotemporal continuity and accuracy of FAPAR products is to take better advantage of the temporal information in the satellite data using deep learning approaches. In this study, the latest version (V6) of the FAPAR product with a 250 m resolution was generated from Moderate Resolution Imaging Spectroradiometer (MODIS) surface reflectance data and other information, as part of the Global LAnd Surface Satellite (GLASS) product suite. In addition, it was aggregated to multiple coarser resolutions (up to 0.25° and monthly). Three existing global FAPAR products (MODIS Collection 6; GLASS V5; and PRoject for On-Board Autonomy–Vegetation, PROBA-V, V1) were used to generate the time-series training samples, which were used to develop a bidirectional long short-term memory (Bi-LSTM) model. Direct validation using high-resolution FAPAR maps from the Validation of Land European Remote sensing Instrument (VALERI) and ImagineS networks revealed that the GLASS V6 FAPAR product has a higher accuracy than PROBA-V, MODIS, and GLASS V5, with an R^2 value of 0.80 and root-mean-square errors (RMSEs) of 0.10–0.11 at the 250 m, 500 m, and 3 km scales, and a higher percentage (72 %) of retrievals for meeting the accuracy requirement of 0.1. Global spatial evaluation and temporal comparison at the AmeriFlux and National Ecological Observatory Network (NEON) sites revealed that the GLASS V6 FAPAR has a greater spatiotemporal continuity and reflects the variations in the vegetation better than the GLASS V5 FAPAR. The higher quality of the GLASS V6 FAPAR is attributed to the ability of the Bi-LSTM model, which involves high-quality training samples and combines the strengths of the existing FAPAR products, as well as the temporal and spectral information from the MODIS surface reflectance data and other information. The 250 m 8 d GLASS V6 FAPAR product for 2020 is freely available at https://doi.org/10.5281/zenodo.6405564 and https://doi.org/10.5281/zenodo.6430925 (Ma, 2022a, b) as well as at the University of Maryland for 2000–2021 (http://glass.umd.edu/FAPAR/MODIS/250m, last access 1 November 2022).

Published by Copernicus Publications.

1 Introduction

Long-term satellite remote sensing observations of terrestrial vegetation are critical for understanding and monitoring climate change. Vegetation influences the global carbon cycle and climate by taking up atmospheric CO_2 through photosynthesis (Knorr et al., 2010). This can be constrained by the energy absorption capacity of the vegetation, and the terrestrial variable related to this process is the fraction of absorbed photosynthetically active radiation (FAPAR). FAPAR is defined as the fraction of the downward surface visible solar radiation (400–700 nm) absorbed by the green elements of plants (Gower et al., 1999). It has been recognized as one of the essential climate variables (GCOS, 2022) and is directly linked to the productivity of vegetation (Kaminski et al., 2012; Mccallum et al., 2009; Smith et al., 2020). FAPAR is not only dependent on the canopy structure, leaf properties, and soil albedo but is also dependent on the illumination conditions. FAPAR under direct illumination is called the black-sky FAPAR, and FAPAR under diffuse illumination is called the white-sky FAPAR (Baret et al., 2013; Liu et al., 2019).

Monitoring changes in the FAPAR using satellites sensors plays an important role in energy balance and carbon cycle modeling. Currently, several global moderate-resolution satellite FAPAR products have been generated and released to the public, including the Sea-viewing Wide Field-of-view Sensor (SeaWiFS) (Gobron et al., 2006), Moderate Resolution Imaging Spectroradiometer (MODIS) (Knyazikhin et al., 1998), Medium Resolution Imaging Spectrometer (MERIS) (Bacour et al., 2006), Geoland2/BioPar version 1 (GEOV1) (Baret et al., 2013), PRoject for On-Board Autonomy–Vegetation (PROBA-V) (Fuster et al., 2020), and Global LAnd Surface Satellite (GLASS) (Liang et al., 2021; Xiao et al., 2015) products. These products have been applied in different research areas such as primary productivity calculations (Zhang et al., 2014), the monitoring of vegetation health (Ivits et al., 2016; Cammalleri et al., 2019; Gobron et al., 2005), crop yield investigations (Dong et al., 2016), and carbon cycle data assimilation in terrestrial ecosystems (Knorr et al., 2010; Smith et al., 2020).

There are two typical types of algorithms for retrieving the FAPAR from satellite data: statistical-model-based and radiative-transfer-model-based algorithms. For example, several studies have estimated FAPAR by establishing the relationship between the vegetation index (VI) and in situ FAPAR measurements using simple statistical methods or machine learning models (Gitelson et al., 2014; Muller et al., 2020; Camacho et al., 2021), while other studies have estimated FAPAR based on energy balance inside the canopy using radiative transfer models (Zhang et al., 2021; Xiao et al., 2015; Liu et al., 2019). Although many satellite products have been generated using these two types of methods, and their accuracies have been evaluated and intercompared in many studies (M. Weiss et al., 2014; Tao et al., 2015; Xiao et al., 2018; Putzenlechner et al., 2019), these algorithms usually only use single-phase remote sensing data, and the critical temporal information contained in the satellite signals is often ignored.

One of the largest problems with the current land surface products is their spatiotemporal inconsistency (Fang et al., 2019; M. Weiss et al., 2014). Owing to the presence of clouds and aerosol contamination in the input observation data, the satellite products usually contain data gaps and outliers, and they are also plagued by a serious lack of data under special geographical and meteorological conditions, such as in tropical forests and high-latitude areas (Camacho et al., 2013). Although many studies have tried to fill these data gaps using either statistical temporal and spatial filtering approaches (D. J. Weiss et al., 2014; Li et al., 2017) or data assimilation methods that exploit dynamic models and ancillary variables (Chernetskiy et al., 2017; Ma et al., 2022), their performance is affected by many factors, such as abrupt land surface changes and cloud cover lasting for a long period of time.

In addition, the targeted FAPAR accuracy and spatial resolution values required by the Global Climate Observing System (GCOS) are 0.05 and 200 m, respectively. However, the global FAPAR product with the highest spatial resolution (300 m) product (i.e., the PROBA-V product) begins in 2014, which cannot meet the requirement for long time-series data in climate change applications. The reported uncertainties of the current FAPAR products vary from 0.08 to 0.23 (Tao et al., 2015; M. Weiss et al., 2014; Pickett-Heaps et al., 2014). Brown et al. (2020) recently evaluated the MODIS, Visible Infrared Imager Radiometer Suite (VIIRS), and PROBA-V FAPAR products over North America and revealed that the PROBA-V product has a higher agreement with field reference data and a better temporal continuity than the MODIS FAPAR and VIIRS FAPAR products. There is an urgent need to develop a 250 m FAPAR product from MODIS surface reflectance data owing to the much longer time period of the MODIS data (i.e., from 2000 to present).

The use of the temporal information contained in the original satellite data, which is ignored by the abovementioned FAPAR estimation algorithms, may be an effective way to improve the spatiotemporal continuity and accuracy of the FAPAR. Recently, by generating a new version of the GLASS leaf area index (LAI) product with a 250 m resolution based on a bidirectional long short-term memory (Bi-LSTM) deep learning approach (Ma and Liang, 2022a), we have demonstrated that the temporal information in satellite observations is extremely useful for generating high-level products with better spatiotemporal continuity and higher accuracy, and the Bi-LSTM model outperforms the general regression neural network (GRNN), LSTM, and gated recurrent unit (GRU) in learning the temporal relationship between satellite surface reflectance and a vegetation variable. To maintain consistency with the GLASS LAI product, in this study, we applied the same strategy to produce a 250 m FAPAR product from MODIS data.

2 Data

2.1 Satellite products

This deep learning approach for FAPAR production capitalizes on the existing global FAPAR products. Three widely used global FAPAR products (MODIS Collection 6, GLASS V5, and PROBA-V1 FAPAR) were fused to generate the true values of the FAPAR time series to create a training dataset.

The MODIS 8 d 500 m FAPAR product (MCD15A2H, Collection 6) was inverted from the MODIS red and near-infrared surface reflectance based on lookup tables simulated using a three-dimensional radiative transfer model for eight biome types. When this main algorithm fails, a backup solution that links the normalized difference vegetation index (NDVI) to FAPAR is adopted (Myneni et al., 2015; Yan et al., 2016). The MODIS FAPAR corresponds to the instantaneous black-sky FAPAR values (i.e., under direct illumination) at 10:30 LST (local solar time). As the MODIS FAPAR is not retrieved over barren, permanent snow- and ice-covered land, the value is set to zero over these non-vegetated pixels. The Copernicus Global Land Service (CGLS) 10 d 300 m PROBA-V FAPAR (V1) is generated from the PROBA-V blue, red, and near-infrared (NIR) surface reflectance data using an artificial neural network (ANN) (Baret et al., 2016). The instantaneous FAPAR is estimated first, and smoothing and gap filling are then applied over a compositing time window. The PROBA-V FAPAR is defined as the instantaneous black-sky FAPAR values (i.e., under direct illumination) at 10:00 LST. The GLASS V5 FAPAR is derived from the GLASS LAI and clumping index products based on the energy balance inside the canopy and soil (Xiao et al., 2015). It mainly considers transmittance of photosynthetically active radiation (PAR) under direct illumination and represents the clear-sky FAPAR at 10:30 LT (local time). Although the FAPAR definitions of the three products are somewhat different, according to previous studies, the impact of these differences on FAPAR's largest difference is less than a few percent compared to the uncertainties of the products (Martínez et al., 2013; Weiss et al., 2007). Thus, the differences in the FAPAR definitions were ignored in this study. In addition, these three products can be used to approximate the daily integrated FAPAR, which is more commonly needed by users than the instantaneous FAPAR. This hypothesis is based on several studies that have reported that the instantaneous FAPAR value at 10:00–10:30 LST (or 14:00–14:30 LST) is very close to the daily average FAPAR value under clear-sky conditions (Baret et al., 2007; Fensholt et al., 2004). Therefore, the goal of this study was to estimate the black-sky FAPAR around 10:30 LST, which is an approximation of the daily average FAPAR.

The 8 d GLASS V6 LAI product was adopted as a potential input feature for the model training, as the LAI has been recognized as one of the most sensitive parameters for FAPAR estimation in previous studies (Xiao et al., 2015; Liu et al., 2019). The 8 d 500 m and 250 m GLASS LAI (V6) were produced from a Bi-LSTM model and from MODIS surface reflectance data. The time series of training samples were generated from three existing LAI products (MODIS, PROBA-V, and GLASS V5) using K-means clustering analysis and the least difference criteria. Direct validation using 79 high-resolution LAI reference maps from three in situ observation networks revealed that the GLASS V6 LAI had the highest accuracy among the current LAI products, with a root-mean-square error (RMSE) of 0.92 at a resolution of 250 m and 0.86 at a resolution of 500 m, while the RMSE of PROBA-V was 0.98 at a resolution of 300 m, and those of GLASS V5 and MODIS C6 were 1.08 and 0.95, respectively, at a resolution of 500 m (Ma and Liang, 2022a).

The MODIS surface reflectance product was used as the observation data for the training of the deep learning model and the FAPAR estimation. In the model training process, as the time series of the 8 d FAPAR samples created from the existing FAPAR products has a 500 m spatial resolution, the 8 d 500 m surface reflectance product (MOD09A1, V6) was used in the model training process. In addition, the 250 m surface reflectance product (MOD09Q1, V6) aims to produce the 250 m FAPAR data and only provides the red and NIR bands at 645 and 858 nm, respectively. Therefore, only the first two red and NIR bands (b1 and b2) and the three solar and satellite angles (solar zenith angle θ_s, view zenith angle θ_v, and relative azimuth angle φ) of MOD09A1 were used in this study.

Although the MODIS surface reflectance has been atmospherically corrected for gases, aerosols, and Rayleigh scattering, residual noise caused by clouds still exists. To remain consistent with the GLASS LAI algorithm, the surface reflectance was not smoothed, and only the pixels with reflectance values outside the $[0, 1]$ range, or without atmospheric correction ($\theta_s > 85°$), were set to zero.

As the MODIS, PROBA-V, and GLASS V5 FAPAR products provide data from 2000, 2014, and 2000 to the present, respectively, the five overlapping years (2014–2018) were selected to generate the global training samples and to test the suitable temporal length for producing the FAPAR. To avoid the invalid values contained in the data samples, FAPAR values outside of the $[0, 1]$ range were set to zero.

2.2 Field FAPAR data

The field FAPAR data used to validate the accuracy of the FAPAR products were collected from 38 sites in the Validation of Land European Remote sensing Instrument (VALERI) (Baret et al., 2005) and ImagineS (Fuster et al., 2020) networks with different land cover types. The ground data were derived from the digital hemispherical photos (DHPs) and represent the fraction of the intercepted PAR (FIPAR), which is considered to be nearly the same as FAPAR (Brown et al., 2020; Weiss et al., 2007). The ground FAPAR measurements were locally regressed using the Landsat or Satellite

Pour l'Observation de la Terre (SPOT) satellite reflectance to generate 62 high-resolution FAPAR reference maps with scales of 20 or 30 m (Table S1 in the Supplement), which were then reprojected onto the MODIS sinusoidal projection and aggregated to 250 and 500 m resolutions to validate the FAPAR products at these resolutions. The high-resolution maps from the Validation of Land European Remote sensing Instrument (VALERI) and ImagineS were also aggregated to a 3 km resolution, and the other field FAPAR values that represent a 3 km area were collected from the DIRECT dataset (Garrigues et al., 2008). A total of 111 reference values were used to validate the FAPAR products at the 3 km resolution. As the field-measured FAPAR is paired with the field-measured LAI, the quality of the field FAPAR was kept consistent with that of the LAI, and the quality was controlled using the relationship between the NDVI and LAI in our previous study (Ma and Liang, 2022a).

To evaluate the temporal consistency of the FAPAR products, we collected the time series of field FAPAR data from two AmeriFlux sites (Novick et al., 2018): the "Bartlett experimental forest site" (US-Bar) and the "Mead-irrigated maize–soybean rotation site" (US-Ne2). The incoming and outgoing flux as well as the flux transmitted through the canopy to the ground were sampled at 30 min intervals, with tower measurement heights of 25 and 5 m for the US-Bar and US-Ne2 sites, respectively. The FAPAR was calculated as the ratio of the measured APAR to the PAR, and the sampled FAPAR values were averaged over the ±30 min time window of the MODIS overpass time (10:30 LT) to produce field FAPAR references for the product comparison. We also used multiyear field measurements (2014–2020) for 10 National Ecological Observatory Network (NEON) sites (Table S2 in the Supplement) for the temporal consistency evaluation of the FAPAR products. This dataset was provided by the Ground-Based Observations for Validation (GBOV) of the Copernicus Global Land Service (https://land.copernicus.eu/global/gbov/, last access: 1 November 2022). The field FAPAR of the NEON sites was derived from the DHPs and represent the instantaneous black-sky FAPAR at 10:00 LT. The spatial representativeness of the NEON sites is about 1.5 km. However, as the AmeriFlux and NEON measurements are tower based, their spatial representativeness is not as explicit as that of the VALERI and ImagineS reference data, so they were only used for intercomparison at the 500 m scale.

3 Methods

The workflow of the algorithm used to generate the 250 m FAPAR is shown in Fig. 1. A deep learning approach that exploits the temporal information in the satellite signals and the current products was adopted to produce the 250 m GLASS V6 FAPAR. The MODIS, GLASS V5, and PROBA-V FAPAR products were used to generate the time series of true values of FAPAR for the global representative sample pixels.

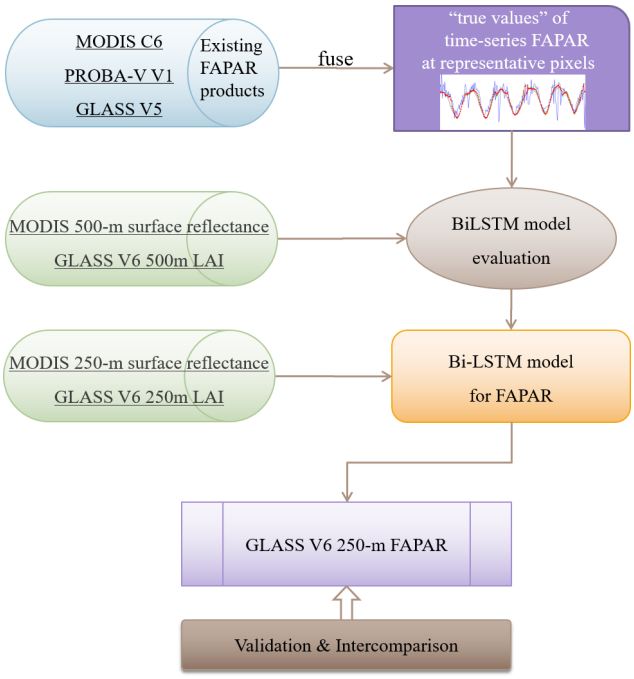

Figure 1. Workflow of the algorithm used to generate the GLASS V6 250 m FAPAR.

The Bi-LSTM model, which was used to produce the GLASS V6 LAI, was used to determine the relationship between the time series of FAPAR and the surface reflectance data.

3.1 Creating global training samples

As FAPAR is physically related to LAI (Mota et al., 2021), the same sample pixels in the GLASS V6 LAI algorithm were used in this study. These globally distributed representative 52 997 sample pixels (Fig. S1 in the Supplement) were selected based on global time-series LAI cluster analysis and the least difference criterion as well as by assuming that the LAI values of the three products with the lowest mean square errors (MSEs) were representative of the true values for a specific pixel (Ma and Liang, 2022a).

In each sample pixel that can represent a time-series profile of the land surface and satellite observation conditions, the differences among the MODIS, PROBA-V, and GLASS V5 FAPARs should be the lowest because the LAIs of these products are the least different. To create the time series of the FAPAR true values, for each 8 d time step from 2014 to 2018, if the difference between the PROBA-V and GLASS V5 FAPARs was less than 0.1, their average was used as the true value; otherwise, the median value of the MODIS, PROBA-V, and GLASS V5 FAPARs was used. As GLASS V5 and PROBA-V FAPAR have relatively smooth temporal profiles because of their pre- or post-process smoothing algorithms, the created FAPAR samples inherited both their smoothness and accuracy at the selected

sample pixels. The histogram distribution of the fused FAPAR values (maximum, average, and all values of the time series) for the representative pixels as well as the GLASS V5, MODIS, and PROBA-V FAPARs for the global land pixels are shown in Fig. 2. Their distributions are quite consistent, indicating that the time series of FAPAR samples are globally representative.

The corresponding 2014–2018 time series of MODIS 500 m surface reflectance (MOD09A1) and the GLASS V6 500 m LAI for the representative pixels were extracted and were used as the control variables of the data samples. We randomly selected 70 % of the samples to train the deep learning model, 20 % to select the optimal deep learning model, and 10 % to evaluate the final model.

3.2 Bi-LSTM model

The Bi-LSTM is a variant of the LSTM and contains forward and backward recurrent net layers (Graves and Schmidhuber, 2005), which are connected to each other and to the output layer. Thus, it can process both the previous and future information of the time series during each time step. The LSTM is involved from the recurrent neural network (RNN), which can process a sequence of data with gaps using its internal memory state. The LSTM is based on its ability to selectively retain or discard relevant information by modulating the information flow using the input, output, and forget gates as well as the cell state (Yildirim, 2018). The structure of the Bi-LSTM has been described by Ma and Liang (2022a).

The structure of the Bi-LSTM model used for the FAPAR estimation had four layers: an input layer, a Bi-LSTM layer with 200 neurons, a dropout layer (5 %), and a regression layer. The Adam optimizer, an initial learning rate of 0.0001, a batch size of 100, and a maximum number of epochs of 100 were set as the parameters for the model training. The time series of the red and NIR reflectance, three angles of the MODIS surface reflectance, and the GLASS V6 500 m LAI were set as the features of the input layer. First, models trained using datasets with two combinations of feature sets (with or without LAI) and a temporal length of 1 year were explored to optimize the input features. Then, the temporal length of the datasets was evaluated to determine the suitable length of the Bi-LSTM model for FAPAR production. Five temporal lengths with a minimum length of 1 year and a maximum length of 5 years were used in this study. The coefficient of determination (R^2), the RMSE, and the bias were used to evaluate the models' performance. Finally, the Bi-LSTM model with the optimal feature set and temporal length was retrained to obtain the final 250 m FAPAR product model.

3.3 Estimating the 250 m resolution FAPAR

The final trained Bi-LSTM model was used to produce FAPAR with an 8 d frequency and 250 m resolution. In line with the model evaluation results (Sect. 4.1), the MODIS 250 m surface reflectance and the GLASS 250 m LAI were used as the input data of the model, and the optimal temporal length used to estimate the FAPAR was determined to be 3 years. Owing to the training error of the model, the derived time series of FAPAR at the connections of two time windows may be discontinuous, and the same post-processing of the GLASS V6 LAI was adopted here. First, the GLASS FAPAR was calculated in the 2000–2002, 2002–2004, …, 2018–2020 time windows, which took about 48 h for a time window using a single graphics processing unit (GPU). As the connection years (2002, 2004, …, 2018) were calculated twice, they were assigned a weight function to obtain the final FAPAR estimates of these years.

The weight function (w) of the GLASS V6 LAI algorithm was adopted:

$$w = \begin{cases} 0 & (1 \le t \le 4) \\ 0.5 \cdot \left(\cos\left(\frac{-\pi \cdot t}{37} + \frac{\pi \cdot 42}{37}\right) + 1\right) & (5 \le t \le 42) \\ 1 & (43 \le t \le 50) \\ 0.5 \cdot \left(\cos\left(\frac{\pi \cdot t}{37} - \frac{\pi \cdot 51}{37}\right) + 1\right) & (51 \le t \le 88) \\ 0 & (89 \le t \le 92). \end{cases} \quad (1)$$

The FAPAR at time step t for the connection or current year (fapar_t) was calculated as follows:

$$\text{fapar}_t = \text{fapar1}_{t+46} \cdot w_{t+46} + \text{fapar2}_t \cdot w_t \quad (1 \le t \le 46), \quad (2)$$

where fapar1 is the time series of FAPAR for the previous and current year, and fapar2 is that for the current and following year. Taking the year 2002 as an example, fapar1 is the time series of FAPAR for 2001–2002, and fapar2 is that for 2002–2003. Because MODIS began collecting data on 24 February 2000, for the 2000–2002 calculation window, the missing data at the beginning days of 2000 were substituted by 2001 to fit the trained model, and the final FAPAR product begins from day of the year (DOY) 57.

3.4 Quality assessment of the GLASS V6 FAPAR product

To quantify the accuracy of the GLASS V6 FAPAR product, we extracted its values in the areas of the corresponding VALERI and ImagineS sites at the original 250 m resolution, and we aggregated them to resolutions of 500 m and 3 km by averaging to enable direct validation at the 250 m, 500 m, and 3 km scales. To compare the three FAPAR products used in this study, the corresponding MODIS, PROBA-V, and GLASS V5 FAPAR values were also extracted and aggregated.

We then assessed the spatial consistency of the GLASS V6 FAPAR product by displaying and analyzing the global distribution of the FAPAR maps in January and July of 2018 as well as two cloud-dominated and two middle- to high-latitude areas: the Yungui district in southwestern China, the

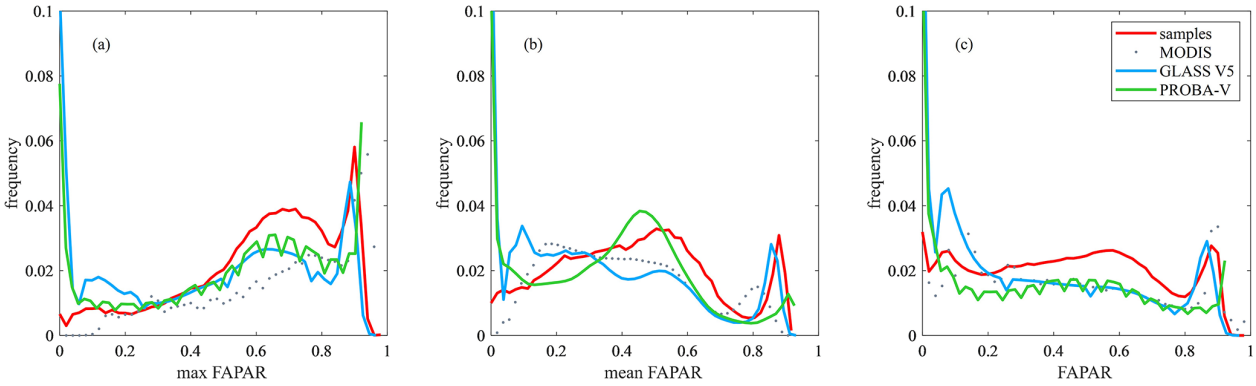

Figure 2. Histogram distribution of the FAPAR values (bin width of 0.02) of the 2014–2018 time series of fused FAPAR samples for the representative pixels and of the MODIS, PROBA-V, and GLASS V5 FAPARs for the global land pixels: **(a)** max FAPAR is the distribution of the maximum FAPAR values of the 2014–2018 time series, **(b)** mean FAPAR is the distribution of the mean FAPAR values of the 2014–2018 time series, and **(c)** FAPAR is the distribution of all of the FAPAR values of the 2014–2018 time series.

Congo Rainforest in central Africa, the central European region, and the Alaskan region. The temporal consistency of the time series of FAPAR from 2000 to 2020 was also assessed at 18 typical sites with representative biome types. Finally, we demonstrated the 2021 8 d time series of FAPAR images at one 1° × 1° cloud-dominated region in southwestern China for the spatiotemporal consistency assessment.

4 Results

4.1 Evaluation of the Bi-LSTM model

The performance of the Bi-LSTM models trained using datasets with two different combinations of feature sets and a length of 1 year are shown in Table 1. The results indicate that incorporating the LAI as one feature of the input improves the accuracy of the model. This finding is consistent with those of many previous studies – that is, the LAI is an important variable for estimating the FAPAR (Tao et al., 2016).

The evaluation results for different temporal lengths are shown in Fig. 3. The RMSE decreases with increasing temporal length from 1 to 5 years for the training, validation, and test datasets. However, the turning point is a length of 3 years, so we set 3 years as the suitable temporal length for the production of the FAPAR. Using the optimal features and temporal length, we retrained the Bi-LSTM model, and the accuracy of the final model is listed in the last row of Table 1.

4.2 Direct validation of FAPAR products

The four FAPAR products were directly validated against field measurements at different scales. The 300 m PROBA-V and 250 m GLASS V6 FAPAR were validated at the 250 m scale; the 500 m MODIS, GLASS V5, and GLASS V6 FAPARs were validated at the 500 m scale; and all four of the

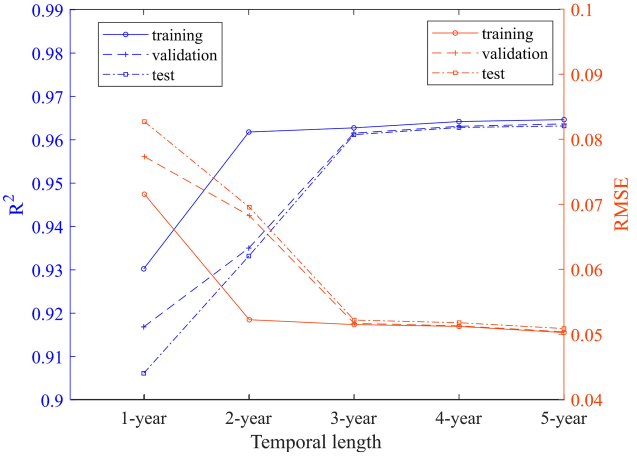

Figure 3. Evaluation of the temporal length of the Bi-LSTM model.

products were aggregated to 3 km and validated at the 3 km scale.

The target accuracy requirement of the GCOS for the global FAPAR product is 0.05; however, meeting this requirement remains a large challenge due to the uncertainties of both the field measurements and the regression-based high-resolution FAPAR reference maps. Therefore, we used the same FAPAR requirement of 0.1 adopted by Brown et al. (2020) to evaluate the PROBA-V FAPAR product, and we denoted a metric P to represent the percentage of pixels meeting the target accuracy requirement in our validation.

The validation results for the PROBA-V and GLASS V6 FAPAR products at the 250 m scale are shown in Fig. 4. Using 23 upscaled high-resolution FAPAR reference maps for 2014 to 2016 obtained from the ImagineS network, the GLASS V6 achieved a slightly higher accuracy than the PROBA-V, with R^2 values of 0.80 and 0.78 and RMSE values of 0.11 and 0.12, respectively. By adding the remaining

Table 1. Accuracies of Bi-LSTM models with different combinations of features.

	Training			Validation			Test		
	R^2	RMSE	Bias	R^2	RMSE	Bias	R^2	RMSE	Bias
b1, b2, θ_s, θ_v, φ	0.955	0.056	0.004	0.953	0.058	0.005	0.952	0.058	0.004
b1, b2, θ_s, θ_v, φ, LAI	0.962	0.051	−0.005	0.962	0.052	−0.005	0.961	0.052	−0.004
Final Bi-LSTM model	0.964	0.050	0.000	0.964	0.050	0.000	0.963	0.051	0.000

39 reference maps from the VALERI network from 2000 to 2013 (the PROBA-V FAPAR is not available during this time period), the RMSE of the GLASS V6 was reduced to 0.10 (Fig. 4c).

The validation results for the MODIS, GLASS V5, and GLASS V6 500 m FAPAR products at the 500 m scale based on 62 upscaled reference FAPAR maps are shown in Fig. 5. The GLASS V6 had the highest accuracy ($R^2 = 0.80$ and RMSE = 0.10), followed by GLASS V5 and MODIS (both $R^2 = 0.69$ and RMSE = 0.13). The MODIS FAPAR had fewer validation points than GLASS FAPAR because of the missing data, and it had the largest bias of 0.07 at these sites. The validation results for the MODIS, GLASS V5, and GLASS V6 FAPAR products at the 3 km scale obtained using the DIRECT dataset for 2000 to 2017 are shown in Fig. 6. The GLASS V6 matched the most data points with the field reference ($N = 111$). Consistent with the 500 m validation results, the GLASS V6 FAPAR had the highest accuracy ($R^2 = 0.81$, RMSE = 0.11).

Table 2 lists the accuracies of each FAPAR product for the different biome types at three scales validated using the reference data from 2000 and 2017, except for PROBA-V (2014–2016). The RMSEs of the GLASS V6 FAPAR are 0.06–0.14, and all of them are less than those of the GLASS V5, MODIS, and PROBA-V at the three scales for the different biome types, except for the shrub and savanna biomes at the 250 m scale.

With respect to assessing the accuracy of the product in terms of meeting the target requirement, the GLASS V6 FAPAR had the highest percentage of pixels with P values greater than 70 % at all three scales, whereas the PROBA-V, MODIS, and GLASS V5 FAPARs had lower percentages, with P values of 54 % to 66 %.

4.3 Spatial consistency evaluation

Examples of the global spatial distributions of the MODIS, PROBA-V, GLASS V5, and GLASS V6 FAPAR products in January and July of 2018 are shown in Fig. 7. The four products were found to have similar spatial consistencies. It should be noted that the gray areas correspond to missing data for the vegetated land surface. The MODIS and PROBA-V FAPARs contain missing data in January in the high-latitude region of the Northern Hemisphere, which is due to cloud/snow contamination or the weak signals of the satellite observations. The GLASS V5 FAPAR cannot provide values above 70°, which is the same as the GLASS V5 LAI, due to the poor representation in these areas during the machine learning model development. GLASS V6 is the only product that provides full land coverage in winter and summer. The first reason for this is that the input GLASS V6 LAI is spatially and temporally continuous globally, and the second is that the Bi-LSTM model can extract the information from the entire time series and assign a value to each time step provided that valid surface reflectance and LAI data are input.

The spatial distributions of the FAPAR products in two cloud-dominated and two middle- to high-latitude regions are shown in Fig. 8. For the Yungui district in southern China, the MODIS and PROBA-V products had large missing data rates of 56 % and 51 %, respectively, whereas the GLASS products were spatially complete. In central Africa, the MODIS product had a missing data rate of 15 %; the PROBA-V product provided more valid data than the MODIS product, but it had lower values compared with the GLASS products. In central Europe, GLASS V6 is more consistent with PROBA-V with respect to textures and values. In Alaska, MODIS contains 17 % data gaps, and PROBA-V exhibits higher FAPAR than others in the lower right regions of Fig. 8d. By comparing the GLASS V5 and V6 products, it was found that V6 was spatially smoother than V5, and it exhibited more details, such as the outline of the river. The reason GLASS V5 contains more noise is that it is based on the traditional surface reflectance filtering process, which inevitably introduces noise and uncertainties, especially in cloud-dominated areas. These cases further confirm that the GLASS V6 product had the highest spatial consistency among the current products in the cloud-dominated areas.

4.4 Temporal consistency evaluation

The time series of the MODIS, PROBA-V, GLASS V5, and GLASS V6 FAPAR products at eight DIRECT and AmeriFlux sites are shown in Fig. 9. The spatial representativeness of the field FAPAR at the DIRECT sites (Fig. 9a–f) is 3 km; therefore, the aggregated 3 km FAPAR products were plotted. As the measurements from the AmeriFlux sites (Fig. 9g–h) are at the tower footprint scale, the corresponding 500 m FAPAR products were extracted and plotted. During

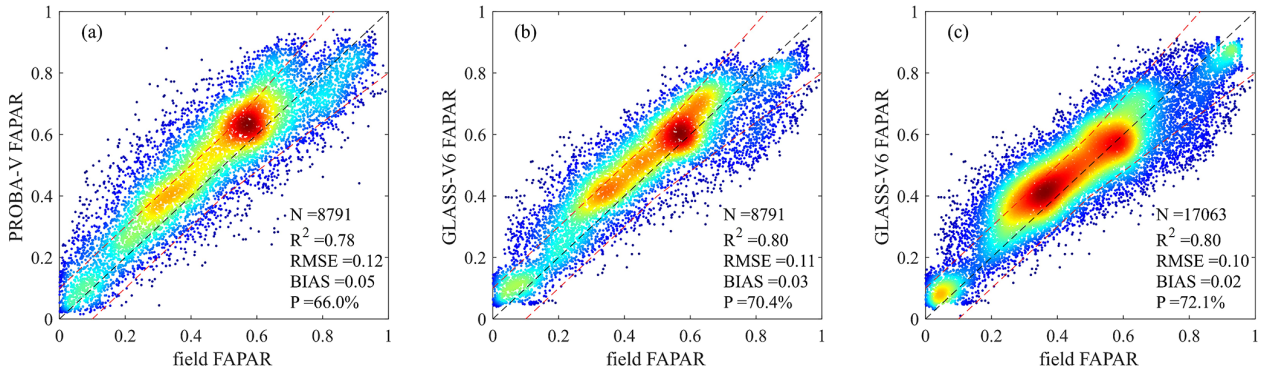

Figure 4. Direct validation of the **(a)** PROBA-V and **(b)** GLASS V6 FAPAR products at the 250 m scale using 23 upscaled high-resolution FAPAR reference maps from 2014 to 2016 from the ImagineS network. **(c)** Direct validation of the GLASS V6 FAPAR product at the 250 m scale using 62 high-resolution FAPAR reference maps from 2000 to 2016 from the Bigfoot, VALERI, and ImagineS networks. The red dashed lines denote the accuracy requirement (P).

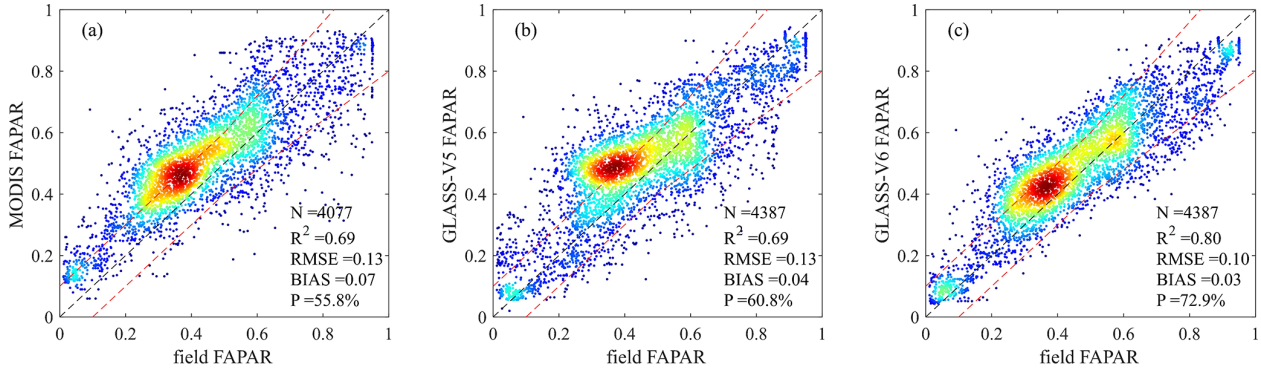

Figure 5. Direct validation of the **(a)** MODIS, **(b)** GLASS V5, and **(c)** GLASS V6 FAPAR products at the 500 m scale using 62 upscaled high-resolution FAPAR reference maps from 2000 to 2016 from the Bigfoot, VALERI, and ImagineS networks.

the growing seasons, the MODIS, PROBA-V, and GLASS products agree well with each other, but the PROBA-V FAPAR has lower values and MODIS has discrete nonstable time series of profiles at the Counami site (Fig. 9b). At the Fundulea cropland site, which has multiple growing seasons, the MODIS, PROBA-V, and GLASS V6 products reflect the multiple growing seasons of the vegetation, while the GLASS V5 product is less sensitive to seasonal variations. At the US-Ne2 cropland and US-Bar forest sites, for which continuous field FAPAR data are available, the four FAPAR products are closer to the field data at the US-Bar site than at the US-Ne2 site. This is due to the spatial representativeness of the tower measurements and the fact that the US-Bar site has a larger footprint and is more homogeneous than the US-Ne2 site (Tao et al., 2015).

The time series of FAPAR of the four products at their original spatial resolutions and the field references at 10 NEON sites are shown in Fig. 10. Generally, the MODIS and GLASS V6 products agree with the field references better than the PROBA-V and GLASS V5 products. At the NEON forest sites, the four products are slightly underestimated compared with the field values. The upper envelope of the MODIS product is closer to the field reference values, but it contains more noise than the other three products. The GLASS V6 FAPAR has more realistic seasonal trends than the V5 product, especially at the site shown in Fig. 10g, where the V5 FAPAR has abnormal seasonality. This is caused by the input of the GLASS V5 LAI data, which have been found to exhibit unrealistic seasonal variations in high-latitude areas. Based on the analysis of the products at these typical sites, the GLASS V6 product was found to have more stable and continuous time-series trends than the other products, and it is an obvious improvement compared with the older version.

The GLASS V6 time series of FAPARs in one $1° \times 1°$ region in southwestern China in 2021 are shown in Fig. 11. The seasonal variations in vegetation FAPAR can be clearly observed, consistent with the previous evaluation results, and the GLASS V6 FAPAR product is spatiotemporally seamless at this cloud-dominated region.

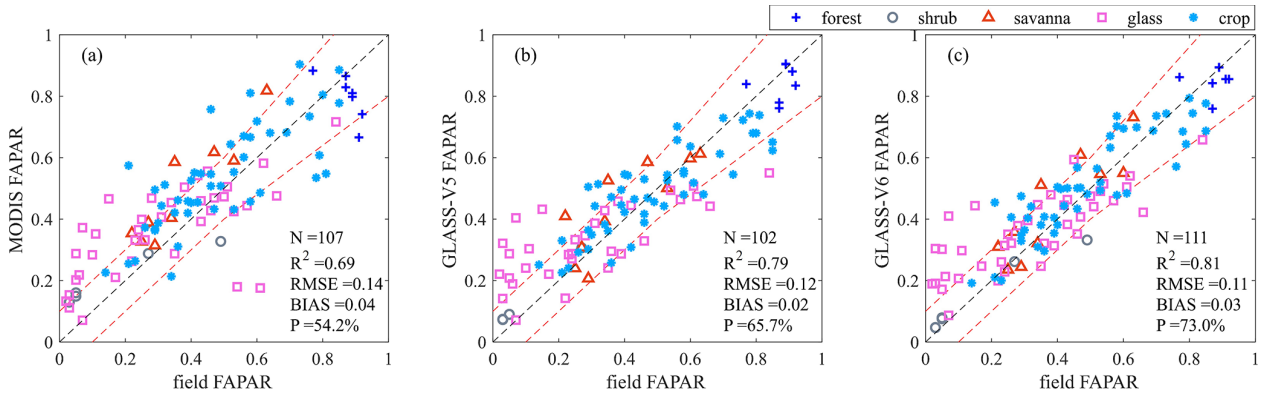

Figure 6. Direct validation of the **(a)** MODIS, **(b)** GLASS V5, and **(c)** GLASS V6 FAPAR products at the 3 km scale using the DIRECT ground measurement dataset from 2000 to 2017.

Table 2. Direct validation of the four FAPAR products at the 250 m, 500 m, and 3 km scales using FAPAR reference maps from 2000 to 2016 for different biome types.

		PROBA-V 250 m	*GLASS V6 250 m	GLASS V6 250 m	MODIS 500 m	GLASS V5 500 m	GLASS V6 500 m	MODIS 3 km	GLASS V5 3 km	GLASS V6 3 km
forest	R^2	0.76	0.90	0.78	0.55	0.59	0.73	0.54	0.05	0.01
	RMSE	0.09	0.09	0.09	0.12	0.11	0.09	0.13	0.07	0.06
	Bias	−0.01	0.06	0.02	0.07	0.05	0.04	−0.08	−0.03	−0.02
	N	415	415	1858	410	432	432	7	7	7
	P	83.9 %	73.3 %	73.8 %	63.9 %	57.6 %	75.9 %	85.7 %	100.0 %	100.0 %
shrub and savanna	R^2	0.49	0.20	0.68	0.62	0.69	0.69	0.81	0.87	0.86
	RMSE	0.09	0.14	0.11	0.10	0.10	0.10	0.12	0.08	0.08
	Bias	−0.03	−0.08	−0.04	0.01	−0.01	−0.04	0.09	0.04	0.02
	N	1137	1137	2249	560	601	601	15	15	16
	P	87.2 %	66.4 %	76.0 %	77.0 %	82.4 %	76.9 %	46.7 %	80.0 %	81.3 %
grass	R^2	0.82	0.87	0.80	0.82	0.67	0.84	0.45	0.56	0.64
	RMSE	0.12	0.10	0.11	0.11	0.13	0.10	0.16	0.15	0.14
	Bias	0.03	0.01	0.00	0.05	0.00	0.01	0.05	0.04	0.04
	N	1381	1381	2065	529	546	546	37	32	40
	P	70.4 %	77.8 %	74.3 %	68.8 %	58.4 %	77.3 %	43.2 %	50.0 %	57.5 %
crop	R^2	0.79	0.83	0.82	0.60	0.64	0.79	0.60	0.72	0.77
	RMSE	0.13	0.10	0.10	0.15	0.13	0.10	0.13	0.10	0.09
	Bias	0.08	0.06	0.04	0.08	0.06	0.04	0.05	0.00	0.02
	N	5858	5858	10891	2460	2678	2678	48	48	48
	P	59.6 %	69.2 %	70.6 %	47.7 %	56.6 %	69.7 %	60.4 %	66.7 %	79.2 %

* GLASS V6 250 m validation results are obtained using the same data points as those used for PROBA-V.

5 Data availability

The 250 m 8 d GLASS V6 FAPAR product for 2020 is freely available at https://doi.org/10.5281/zenodo.6405564 and https://doi.org/10.5281/zenodo.6430925 (Ma, 2022a, b) as well as at the University of Maryland for 2000–2021 (http://glass.umd.edu/FAPAR/MODIS/250m, last access 1 November 2022, Ma and Liang, 2022b). We have also aggregated it to coarser resolutions (500 m 8 d, 0.05° 8 d, 0.1° per month, and 0.25° per month; http://glass.umd.edu/FAPAR/MODIS/, last access: 1 November 2022, Ma, and Liang, 2022c). The 250 and 500 m data are in the sinusoidal projection, whereas the 0.05, 0.1, and 0.25° data are in the geographic latitude and longitude coordinate system. The data files are provided in Hierarchical Data Format – Earth Observing Systems (HDF-EOS) format.

The GLASS V6 LAI dataset was downloaded from http://www.glass.umd.edu/LAI/MODIS/250m/ (last access: 1 November 2022, Ma, and Liang, 2022d). The MODIS and PROBA-V products were downloaded from https://earthdata.

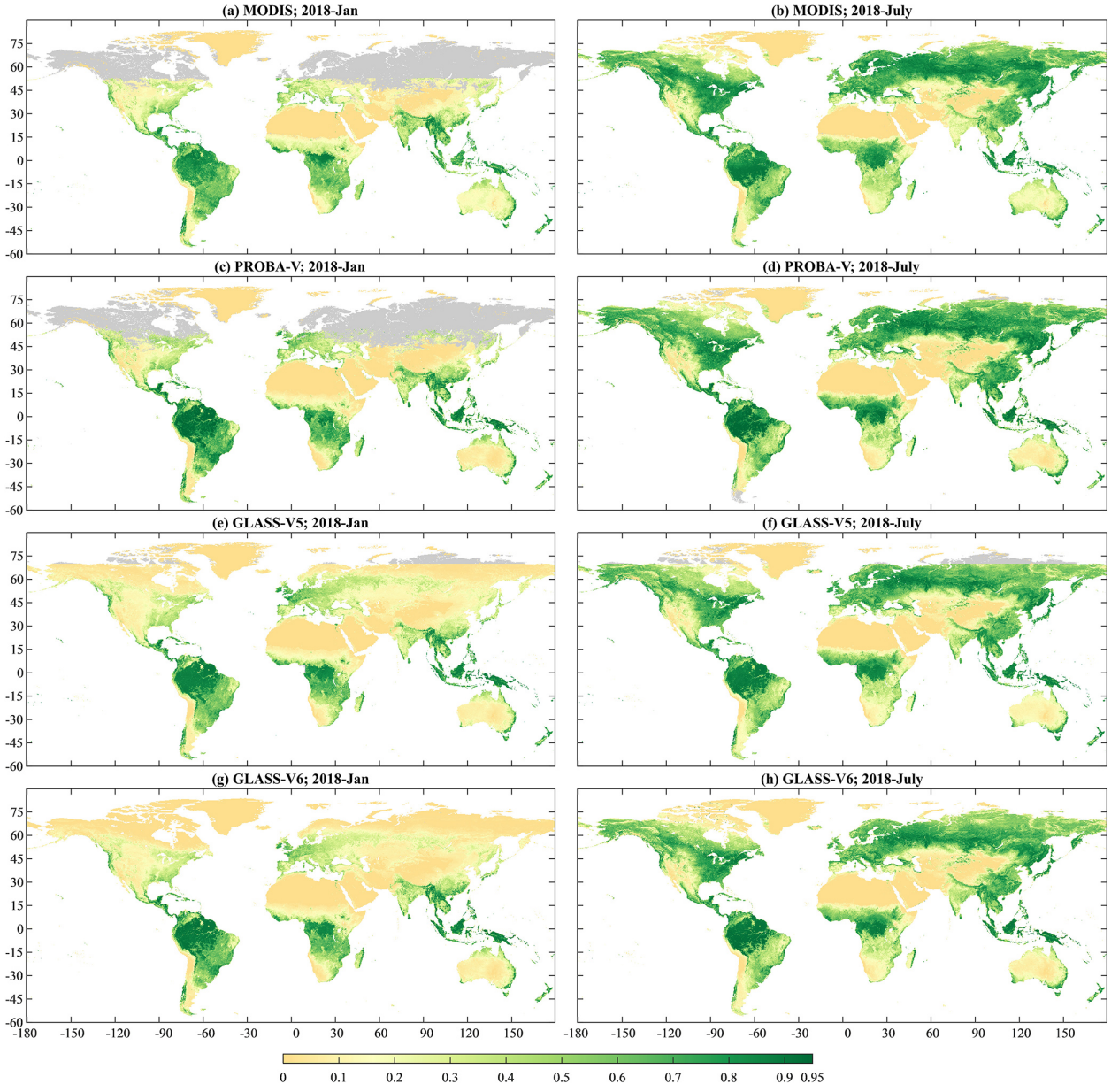

Figure 7. Global spatial distributions of the MODIS, PROB-V, GLASS V5, and GLASS V6 FAPARs in January and July of 2018: **(a)** MODIS, January 2018; **(b)** MODIS, July 2018; **(c)** PROBA-V, January 2018; **(d)** PROBA-V, July 2018; **(e)** GLASS V5, January 2018; **(f)** GLASS V5, July 2018; **(g)** GLASS V6, January 2018; and **(h)** GLASS V6, July 2018. The spatial resolution is 0.05° latitude and longitude.

nasa.gov/ (last access: 1 November 2022) and https://land.copernicus.eu/global/products/fapar (last access: 1 November 2022), respectively.

6 Conclusions

In this study, the GLASS FAPAR product with a 250 m spatial resolution was derived from MODIS surface reflectance data. To our knowledge, this is the global long-time-series FAPAR product for 2000–2021 with the highest spatial resolution. The time series of FAPAR samples used for the model training were created by merging the existing MODIS, PROBA-V, and GLASS V5 FAPAR products using globally distributed representative samples. The red and NIR bands; the solar zenith, view zenith, and relative azimuth angles obtained from the 250 m MODIS surface reflectance product; and the 250 m GLASS LAI data were used as the features to predict the FAPAR values. The time series of GLASS V6 FAPAR was generated using the trained model at an optimal temporal length of 3 years. The accuracy and spatiotemporal consistency of the GLASS V6 FAPAR was quantified and evaluated through validation against field reference

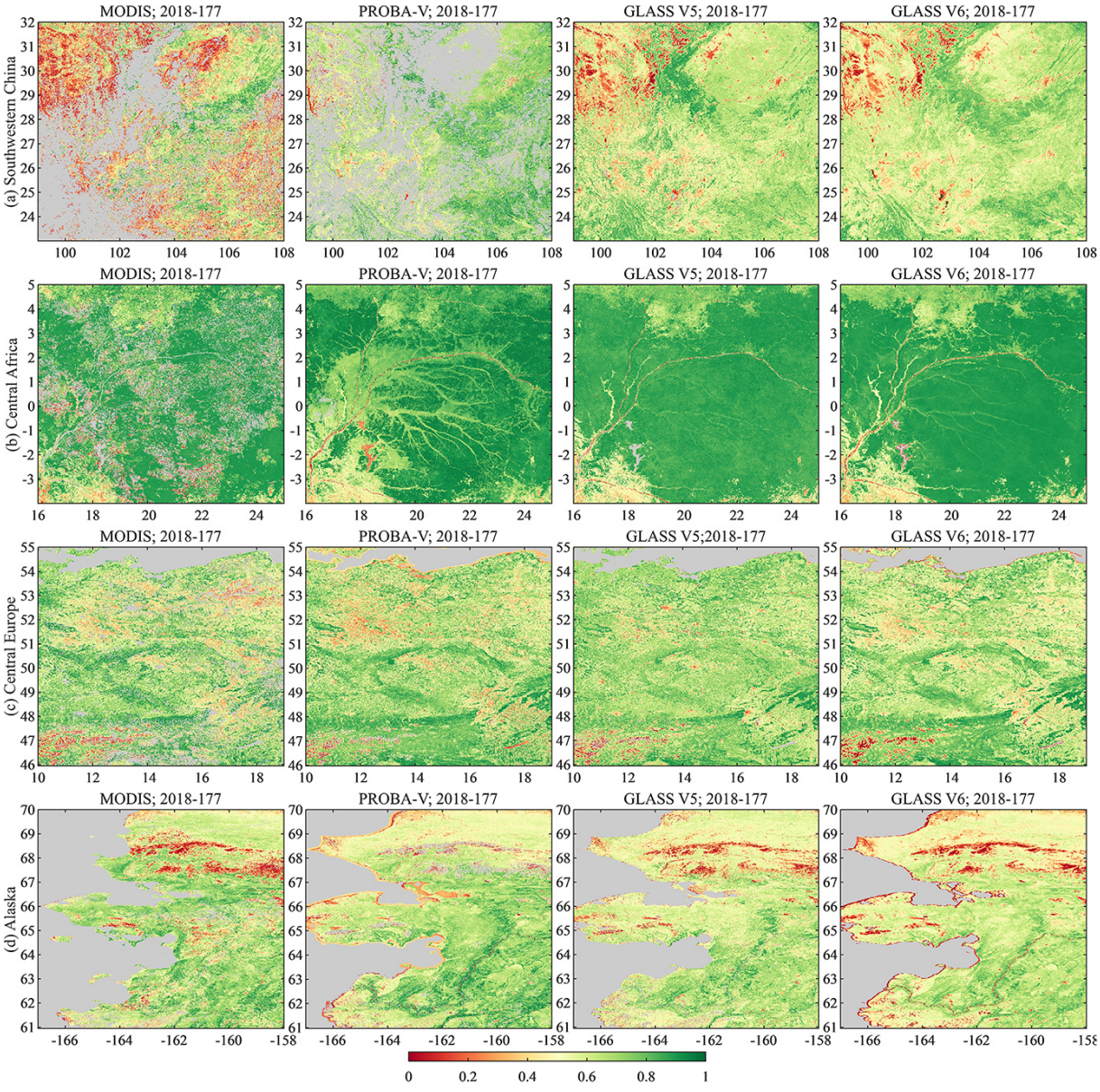

Figure 8. Spatial distribution of MODIS, PROB-V, GLASS V5, and V6 FAPARs on DOY 177 in 2018 in four regions: **(a)** the Yungui district in southwestern China; **(b)** the Congo Rainforest in central Africa; **(c)** central Europe; and **(d)** Alaska. The spatial resolution is 500 m latitude and longitude.

data and was compared with the MODIS, PROBA-V, and GLASS V5 FAPAR products. Through validation using 62 high-resolution FAPAR reference maps from the VALERI and ImagineS networks and 111 reference values from DIRECT, the GLASS V6 FAPAR product was demonstrated to have the best agreement with the reference data, with an R^2 value of 0.80 and RMSEs of 0.10–0.11 at the 250 m, 500 m, and 3 km scales, and the highest percentage (72 %) of retrievals in terms of meeting the accuracy requirements. In terms of the spatiotemporal consistency evaluation, the GLASS V6 FAPAR was demonstrated to have global coverage without missing data, maintain high quality even in cloud-dominated areas, exhibit consistent temporal profiles, and reflect the seasonal variations in the vegetation well.

The GLASS V6 FAPAR product is the first global long-term FAPAR product with a resolution of 250 m. The higher quality of the GLASS V6 FAPAR is attributed to the ability of the Bi-LSTM model to exploit the advantages of the existing FAPAR products as well as to extract the temporal and spectral information from the MODIS observations and the GLASS LAI product. However, the accuracy still needs to be improved to fully meet the GCOS accuracy re-

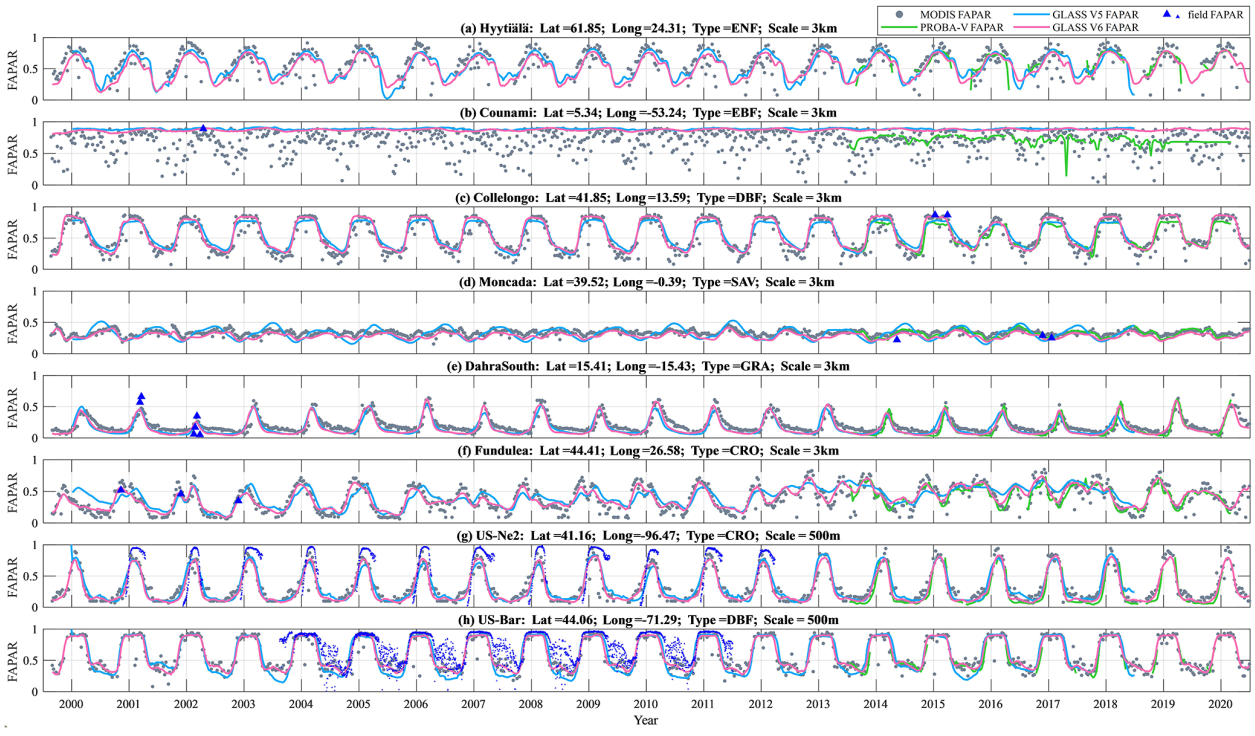

Figure 9. **(a–f)** Aggregated 3 km time series of MODIS, GLASS V5, GLASS V6, and PROBA-V FAPAR products at six DIRECT sites with different types of biomes during 2000–2020 and **(g–h)** 500 m time series of FAPAR products at two AmeriFlux sites.

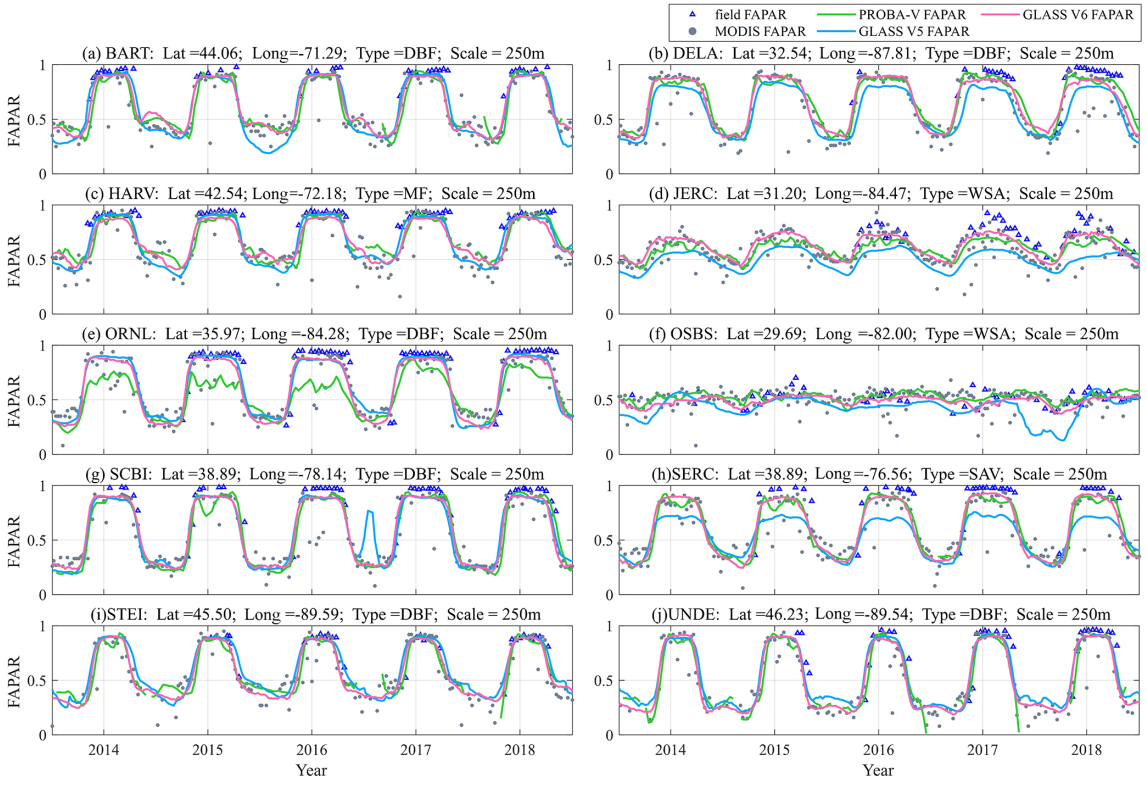

Figure 10. Time series of FAPARs from the MODIS 500 m, GLASS V5 500 m, GLASS V6 250 m, and PROBA-V 300 m products at 10 NEON sites during 2014–2018.

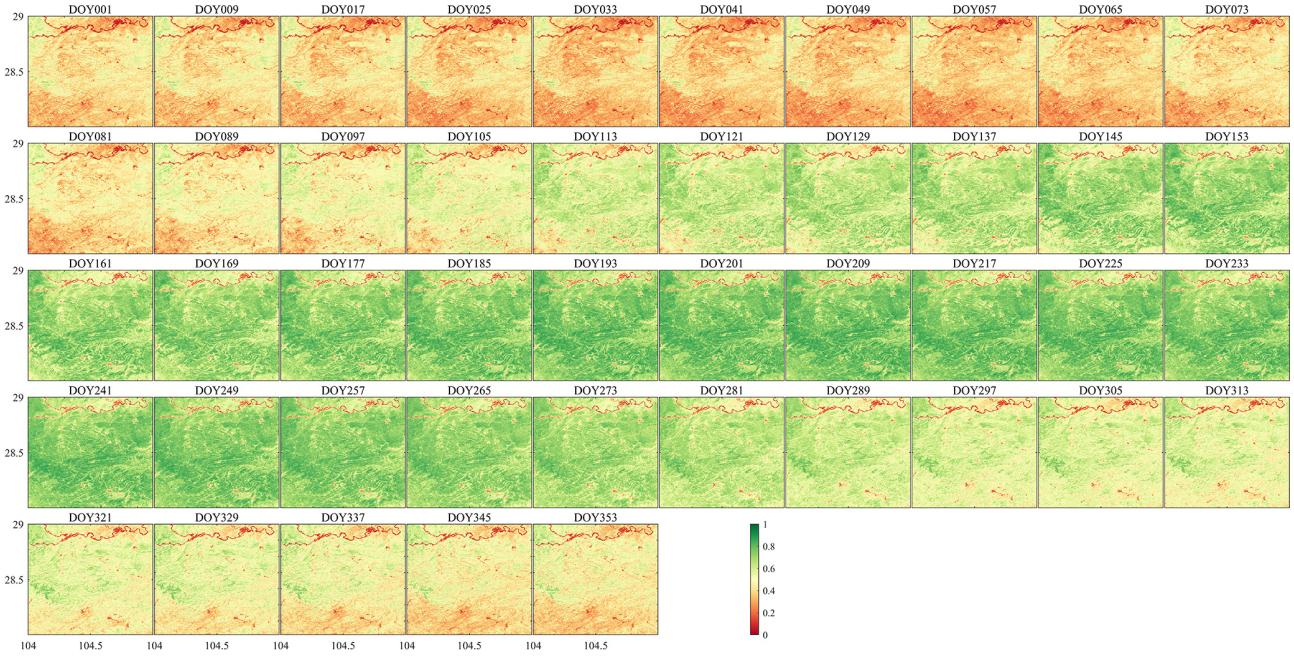

Figure 11. GLASS V6 time series of FAPARs in a 1° × 1° region in southwestern China in 2021. The spatial resolution is 250 m latitude and longitude.

quirements. One source of uncertainty is related to the differences between the FAPAR definitions of the three FAPAR datasets used in the model training process. These differences may lead to a slight uncertainty, which was not explicitly accounted for. More ground measurements for different ecosystems under various conditions are needed to further evaluate the FAPAR product.

Supplement. The supplement related to this article is available online at: https://doi.org/10.5194/essd-14-5333-2022-supplement.

Author contributions. HM performed the data curation, investigation, methodology, validation, and wrote the original draft of the paper. SL was responsible for conceptualization, supervision, and reviewed and edited the manuscript. CX and BL contributed to the data resources and validation. QW and AJ participated in data production and distribution.

Competing interests. The contact author has declared that none of the authors has any competing interests.

Disclaimer. Publisher's note: Copernicus Publications remains neutral with regard to jurisdictional claims in published maps and institutional affiliations.

Acknowledgements. The authors would like to thank the principal investigators of the VALERI, ImagineS, and NEON networks for providing FAPAR reference data. We are also very grateful to Francesco N. Tubiello and the reviewers for their valuable comments and suggestions.

Financial support. This research has been supported by the National Natural Science Foundation of China (grant no. 42090011).

Review statement. This paper was edited by Francesco N. Tubiello and reviewed by two anonymous referees.

References

Bacour, C., Baret, F., Beal, D., Weiss, M., and Pavageau, K.: Neural network estimation of LAI, fAPAR, fCover and LAI×C ab, from top of canopy MERIS reflectance data: Principles and validation, Remote Sens. Environ., 105, 313–325, 2006.

Baret, F., Weiss, M., Allard, D., Garrigues, S., Leroy, M., Jeanjean, H., Fernandes, R., Myneni, R., Privette, J., and Morisette, J.: VALERI: a network of sites and a methodology for the validation of medium spatial resolution land satellite productss, ffhal-03221068, https://hal.archives-ouvertes.fr/hal-03221068/ (last access 1 November 2022), 2021.

Baret, F., Hagolle, O., Geiger, B., Bicheron, P., Miras, B., Huc, M., Berthelot, B., Niño, F., Weiss, M., and Samain, O.: LAI, fAPAR and fCover CYCLOPES global products derived from VEGETATION: Part 1: Principles of the algorithm, Remote Sens. Environ., 110, 275–286, 2007.

Baret, F., Weiss, M., Lacaze, R., Camacho, F., Makhmara, H., Pacholcyzk, P., and Smets, B.: GEOV1: LAI and FAPAR essential climate variables and FCOVER global time series capitalizing over existing products. Part 1: Principles of development and production, Remote Sens. Environ., 137, 299–309, https://doi.org/10.1016/j.rse.2012.12.027, 2013.

Baret, F., Weiss, M., Verger, A., and Smets, B.: ATBD For LAI, FAPAR And FCOVER From PROBA-V Products At 300 m Resolution (GEOV3), Imagines_rp2.1_atbd-lai, 300, https://land.copernicus.eu/global/sites/cgls.vito.be/files/products/ImagineS_RP2.1_ATBD-LAI300m_I1.73.pdf, (last access 1 November 2022), 2016.

Brown, L. A., Meier, C., Morris, H., Pastor-Guzman, J., Bai, G., Lerebourg, C., Gobron, N., Lanconelli, C., Clerici, M., and Dash, J.: Evaluation of global leaf area index and fraction of absorbed photosynthetically active radiation products over North America using Copernicus Ground Based Observations for Validation data, Remote Sens. Environ., 247, 111935, https://doi.org/10.1016/j.rse.2020.111935, 2020.

Camacho, F., Cernicharo, J., Lacaze, R., Baret, F., and Weiss, M.: GEOV1: LAI, FAPAR essential climate variables and FCOVER global time series capitalizing over existing products. Part 2: Validation and intercomparison with reference products, Remote Sens. Environ., 137, 310–329, 2013.

Camacho, F., Fuster, B., Li, W., Weiss, M., Ganguly, S., Lacaze, R., and Baret, F.: Crop specific algorithms trained over ground measurements provide the best performance for GAI and fAPAR estimates from Landsat-8 observations, Remote Sens. Environ., 260, 112453, https://doi.org/10.1016/j.rse.2021.112453, 2021.

Cammalleri, C., Verger, A., Lacaze, R., and Vogt, J. V.: Harmonization of GEOV2 fAPAR time series through MODIS data for global drought monitoring, Int. J. Appl. Earth Obs., 80, 1–12, https://doi.org/10.1016/j.jag.2019.03.017, 2019.

Chernetskiy, M., Gómez-Dans, J., Gobron, N., Morgan, O., Lewis, P., Truckenbrodt, S., and Schmullius, C.: Estimation of FAPAR over croplands using MISR data and the earth observation land data assimilation system (EO-LDAS), Remote Sens.-Basel, 9, 656, 2017.

Dong, T., Liu, J., Shang, J., Qian, B., Huffman, T., Zhang, Y., Champagne, C., and Daneshfar, B.: Assessing the Impact of Climate Variability on Cropland Productivity in the Canadian Prairies Using Time Series MODIS FAPAR, Remote Sens.-Basel, 8, 281, https://doi.org/10.3390/rs8040281, 2016.

Fang, H., Baret, F., Plummer, S., and Schaepman-Strub, G.: An Overview of Global Leaf Area Index (LAI): Methods, Products, Validation, and Applications, Rev. Geophys., 57, 739–799, https://doi.org/10.1029/2018RG000608, 2019.

Fensholt, R., Sandholt, I., and Rasmussen, M. S.: Evaluation of MODIS LAI, fAPAR and the relation between fAPAR and NDVI in a semi-arid environment using in situ measurements, Remote Sens. Environ., 91, 490–507, 2004.

Fuster, B., Sánchez-Zapero, J., Camacho, F., García-Santos, V., Verger, A., Lacaze, R., Weiss, M., Baret, F., and Smets, B.: Quality Assessment of PROBA-V LAI, fAPAR and fCOVER Collection 300 m Products of Copernicus Global Land Service, Remote Sens.-Basel, 12, 1017, https://doi.org/10.3390/rs12061017, 2020.

Garrigues, S., Lacaze, R., Baret, F., Morisette, J., Weiss, M., Nickeson, J., Fernandes, R., Plummer, S., Shabanov, N., and Myneni, R.: Validation and intercomparison of global Leaf Area Index products derived from remote sensing data, J. Geophys. Res.-Biogeo., 113, G02028, 2008.

GCOS: The 2022 GCOS Implementation Plan, GCOS-244, GOOS-272, https://library.wmo.int/doc_num.php?explnum_id=11317, last access: 1 November 2022.

Gitelson, A. A., Peng, Y., and Huemmrich, K. F.: Relationship between fraction of radiation absorbed by photosynthesizing maize and soybean canopies and NDVI from remotely sensed data taken at close range and from MODIS 250 m resolution data, Remote Sens. Environ., 147, 108–120, https://doi.org/10.1016/j.rse.2014.02.014, 2014.

Gobron, N., Pinty, B., Mélin, F., Taberner, M., Verstraete, M., Belward, A., Lavergne, T., and Widlowski, J. L.: The state of vegetation in Europe following the 2003 drought, Int. J. Remote Sens., 26, 2013–2020, 2005.

Gobron, N., Pinty, B., Aussedat, O., Chen, J. M., Cohen, W. B., Fensholt, R., Gond, V., Huemmrich, K. F., Lavergne, T., and Mélin, F.: Evaluation of fraction of absorbed photosynthetically active radiation products for different canopy radiation transfer regimes: Methodology and results using Joint Research Center products derived from SeaWiFS against ground-based estimations, J. Geophys. Res.-Atmos., 111, D13110, 2006.

Gower, S. T., Kucharik, C. J., and Norman, J. M.: Direct and indirect estimation of leaf area index, fAPAR, and net primary production of terrestrial ecosystems, Remote Sens. Environ., 70, 29–51, 1999.

Graves, A. and Schmidhuber, J.: Framewise phoneme classification with bidirectional LSTM and other neural network architectures, Neural Networks, 18, 602–610, 2005.

Ivits, E., Horion, S., Erhard, M., and Fensholt, R.: Assessing European ecosystem stability to drought in the vegetation growing season, Global Ecol. Biogeogr., 25, 1131–1143, 2016.

Kaminski, T., Knorr, W., Scholze, M., Gobron, N., Pinty, B., Giering, R., and Mathieu, P.-P.: Consistent assimilation of MERIS FAPAR and atmospheric CO_2 into a terrestrial vegetation model and interactive mission benefit analysis, Biogeosciences, 9, 3173–3184, https://doi.org/10.5194/bg-9-3173-2012, 2012.

Knorr, W., Kaminski, T., Scholze, M., Gobron, N., Pinty, B., Giering, R., and Mathieu, P.-P.: Carbon cycle data assimilation with a generic phenology model, J. Geophys. Res.-Biogeo., 115, G04017, https://doi.org/10.1029/2009JG001119, 2010.

Knyazikhin, Y., Martonchik, J., Myneni, R., Diner, D., and Running, S.: Synergistic algorithm for estimating vegetation canopy leaf area index and fraction of absorbed photosynthetically active radiation from MODIS and MISR data, J. Geophys. Res.-Atmos., 103, 32257–32275, 1998.

Li, W., Baret, F., Weiss, M., Buis, S., Lacaze, R., Demarez, V., Dejoux, J.-F., Battude, M., and Camacho, F.: Combining hectometric and decametric satellite observations to provide near real time decametric FAPAR product, Remote Sens. Environ., 200, 250–262, https://doi.org/10.1016/j.rse.2017.08.018, 2017.

Liang, S., Cheng, J., Jia, K., Jiang, B., Liu, Q., Xiao, Z., Yao, Y., Yuan, W., Zhang, X., and Zhao, X.: The global Land surface satellite (GLASS) product suite, B. Am. Meteorol. Soc., 102, E323–E337, 2021.

Liu, L., Zhang, X., Xie, S., Liu, X., Song, B., Chen, S., and Peng, D.: Global White-Sky and Black-Sky FAPAR Retrieval Using the Energy Balance Residual Method: Algorithm and Validation, Re-

mote Sens.-Basel, 11, 1004, https://doi.org/10.3390/rs11091004, 2019.

Ma, H.: A global land surface 250-m 8-day Fraction of Absorbed Photosynthetically Active Radiation (FAPAR) product (2022-part1) (V006), Zenodo [data set], https://doi.org/10.5281/zenodo.6405564, 2022a.

Ma, H.: A global land surface 250-m 8-day Fraction of Absorbed Photosynthetically Active Radiation (FAPAR) product (2022-part2) (V006) Zenodo [data set], https://doi.org/10.5281/zenodo.6430925, 2022b.

Ma, H. and Liang, S.: Development of the GLASS 250-m leaf area index product (version 6) from MODIS data using the bidirectional LSTM deep learning model, Remote Sens. Environ., 273, 112985, https://doi.org/10.1016/j.rse.2022.112985, 2022a.

Ma, H., and Liang, S.: GLASS 250m V6 FAPAR [data set], http://glass.umd.edu/FAPAR/MODIS/250m, last access 1 November 2022b.

Ma, H., and Liang, S.: GLASS 500m , 0.05° , and 0.1° FAPAR [data set], http://glass.umd.edu/FAPAR/MODIS/, last access: 1 November 2022c.

Ma, H., and Liang, S.: GLASS 250m V6 LAI [data set], http://www.glass.umd.edu/LAI/MODIS/250m/, last access: 1 November 2022d.

Ma, H., Liang, S., Zhu, Z., and He, T.: Developing a Land Continuous Variable Estimator to Generate Daily Land Products From Landsat Data, IEEE T. Geosci. Remote, 60, 1–19, https://doi.org/10.1109/TGRS.2021.3121272, 2022.

Martínez, B., Camacho, F., Verger, A., García-Haro, F. J., and Gilabert, M.: Intercomparison and quality assessment of MERIS, MODIS and SEVIRI FAPAR products over the Iberian Peninsula, Int. J. Appl. Earth Obs., 21, 463–476, 2013.

McCallum, I., Wagner, W., Schmullius, C., Shvidenko, A., Obersteiner, M., Fritz, S., and Nilsson, S.: Satellite-based terrestrial production efficiency modeling, Carbon Balance and Management, 4, 1–14, 2009.

Mota, B., Gobron, N., Morgan, O., Cappucci, F., Lanconelli, C., and Robustelli, M.: Cross-ECV consistency at global scale: LAI and FAPAR changes, Remote Sens. Environ., 263, 112561, https://doi.org/10.1016/j.rse.2021.112561, 2021.

Muller, S. J., Sithole, P., Singels, A., and Van Niekerk, A.: Assessing the fidelity of Landsat-based fAPAR models in two diverse sugarcane growing regions, Comput. Electron. Agr., 170, 105248, https://doi.org/10.1016/j.compag.2020.105248, 2020.

Myneni, R., Knyazikhin, Y., and Park, T.: MOD15A2H MODIS/Terra Leaf Area Index/FPAR 8-Day L4 Global 500 m SIN Grid V006, NASA EOSDIS Land Processes DAAC, https://doi.org/10.5067/MODIS/MOD15A2H.006, 2015.

Novick, K. A., Biederman, J., Desai, A., Litvak, M., Moore, D. J., Scott, R., and Torn, M.: The AmeriFlux network: A coalition of the willing, Agr. Forest Meteorol., 249, 444–456, 2018.

Pickett-Heaps, C. A., Canadell, J. G., Briggs, P. R., Gobron, N., Haverd, V., Paget, M. J., Pinty, B., and Raupach, M. R.: Evaluation of six satellite-derived Fraction of Absorbed Photosynthetic Active Radiation (FAPAR) products across the Australian continent, Remote Sens. Environ., 140, 241–256, https://doi.org/10.1016/j.rse.2013.08.037, 2014.

Putzenlechner, B., Castro, S., Kiese, R., Ludwig, R., Marzahn, P., Sharp, I., and Sanchez-Azofeifa, A.: Validation of Sentinel-2 fAPAR products using ground observations across three forest ecosystems, Remote Sens. Environ., 232, 111310, https://doi.org/10.1016/j.rse.2019.111310, 2019.

Smith, W. K., Fox, A. M., MacBean, N., Moore, D. J. P., and Parazoo, N. C.: Constraining estimates of terrestrial carbon uptake: new opportunities using long-term satellite observations and data assimilation, New Phytol., 225, 105–112, https://doi.org/10.1111/nph.16055, 2020.

Tao, X., Liang, S., and Wang, D.: Assessment of five global satellite products of fraction of absorbed photosynthetically active radiation: Intercomparison and direct validation against ground-based data, Remote Sens. Environ., 163, 270–285, https://doi.org/10.1016/j.rse.2015.03.025, 2015.

Tao, X., Liang, S., He, T., and Jin, H.: Estimation of fraction of absorbed photosynthetically active radiation from multiple satellite data: Model development and validation, Remote Sens. Environ., 184, 539–557, https://doi.org/10.1016/j.rse.2016.07.036, 2016.

Weiss, D. J., Atkinson, P. M., Bhatt, S., Mappin, B., Hay, S. I., and Gething, P. W.: An effective approach for gap-filling continental scale remotely sensed time-series, ISPRS J. Photogramm., 98, 106–118, https://doi.org/10.1016/j.isprsjprs.2014.10.001, 2014.

Weiss, M., Baret, F., Garrigues, S., and Lacaze, R.: LAI and fAPAR CYCLOPES global products derived from VEGETATION. Part 2: validation and comparison with MODIS collection 4 products, Remote Sens. Environ., 110, 317–331, 2007.

Weiss, M., Baret, F., Block, T., Koetz, B., Burini, A., Scholze, B., Lecharpentier, P., Brockmann, C., Fernandes, R., and Plummer, S.: On Line Validation Exercise (OLIVE): A web based service for the validation of medium resolution land products. Application to FAPAR products, Remote Sens.-Basel, 6, 4190–4216, 2014.

Xiao, Z., Liang, S., Sun, R., Wang, J., and Jiang, B.: Estimating the fraction of absorbed photosynthetically active radiation from the MODIS data based GLASS leaf area index product, Remote Sens. Environ., 171, 105–117, https://doi.org/10.1016/j.rse.2015.10.016, 2015.

Xiao, Z., Liang, S., and Sun, R.: Evaluation of three long time series for global fraction of absorbed photosynthetically active radiation (fapar) products, IEEE T. Geosci. Remote, 56, 5509–5524, 2018.

Yan, K., Park, T., Yan, G., Chen, C., Yang, B., Liu, Z., Nemani, R. R., Knyazikhin, Y., and Myneni, R. B.: Evaluation of MODIS LAI/FPAR product collection 6. Part 1: Consistency and improvements, Remote Sens.-Basel, 8, 359, 2016.

Yildirim, Ö.: A novel wavelet sequence based on deep bidirectional LSTM network model for ECG signal classification, Comput. Biol. Med., 96, 189–202, 2018.

Zhang, Q., Cheng, Y.-B., Lyapustin, A. I., Wang, Y., Gao, F., Suyker, A., Verma, S., and Middleton, E. M.: Estimation of crop gross primary production (GPP): fAPARchl versus MOD15A2 FPAR, Remote Sens. Environ., 153, 1–6, 2014.

Zhang, Y., Fang, H., Wang, Y., and Li, S.: Variation of intra-daily instantaneous FAPAR estimated from the geostationary Himawari-8 AHI data, Agr. Forest Meteorol., 307, 108535, https://doi.org/10.1016/j.agrformet.2021.108535, 2021.